electronics

MDPI

Article

A Multiplier-Free Dual-Hadamard Architecture for Peak-to-Average Power Ratio Reduction in OFDM Systems

Mengwan Jiang [1,*], Yusheng Mei [2], Minchen Shi [2] and Dejin Kong [2]

[1] School of Artificial Intelligence and Big Data, Henan University of Technology, Zhengzhou 450001, China
[2] School of Electronic and Electrical Engineering, Wuhan Textile University, Wuhan 430200, China; 2415363038@wtu.edu.cn (Y.M.); 2415363060@wtu.edu.cn (M.S.); djkou@wtu.edu.cn (D.K.)
* Correspondence: jiangmw@haut.edu.cn

Abstract

Orthogonal frequency division multiplexing (OFDM) is widely used in broadband wireless communication systems because of its high spectral efficiency, flexible subcarrier allocation, and robustness against frequency-selective fading. However, the high peak-to-average power ratio (PAPR) of OFDM signals reduces the power efficiency of high-power amplifiers and may introduce nonlinear distortion. To address this problem, this paper proposes a multiplier-free Dual-Hadamard PAPR-reduction architecture. The term multiplier-free refers to the additional precoding and phase-weighting operations introduced by the proposed PAPR reduction module, excluding the common OFDM FFT/IFFT operations. Specifically, the proposed architecture combines fast Walsh–Hadamard transform (FWHT) precoding, interleaved partitioning (ILP), and Hadamard-based partial transmit sequence (H-PTS) weighting. Since the FWHT matrix and the H-PTS phase codebook contain only binary signs, the main additional operations are implemented by additions, subtractions, and sign inversions. Simulation results demonstrate that the proposed method reduces the PAPR relative to conventional OFDM without degrading the system's bit error rate (BER) performance in an additive white Gaussian noise (AWGN) channel when the side information is recovered correctly.

Keywords: OFDM; peak-to-average power ratio; Walsh–Hadamard transform; partial transmit sequence; multiplier-free architecture; interleaved partitioning; IoT

1. Introduction

Orthogonal frequency division multiplexing (OFDM) remains a key multicarrier waveform in broadband wireless systems because it provides high spectral efficiency, flexible subcarrier allocation, and robustness against frequency-selective fading. These advantages are still relevant in the evolution from 5G-Advanced to IMT-2030/6G, where high data rates, dense connectivity, sensing-assisted services, and energy-efficient terminals are expected to coexist [1–4]. In Internet-of-Things (IoT) and compact radio nodes, the transmitter is often constrained by power consumption, circuit area, and implementation cost [5]. Therefore, waveform-processing methods that reduce transmitter power-amplifier stress while maintaining simple hardware are of practical importance.

Despite its advantages, OFDM has an intrinsic physical-layer drawback: a high peak-to-average power ratio (PAPR). Since the time-domain OFDM signal is generated by summing many independently modulated subcarriers, constructive superposition may produce large envelope peaks [6]. A high PAPR forces a high-power amplifier (HPA) to

Check for updates

Academic Editor: Hung-Yu Chien

Received: 29 April 2026
Revised: 8 July 2026
Accepted: 10 July 2026
Published: 14 July 2026

Copyright: © 2026 by the authors. Licensee MDPI, Basel, Switzerland. This article is an open access article distributed under the terms and conditions of the Creative Commons Attribution (CC BY) license.

operate with a larger input back-off in order to avoid nonlinear distortion. However, this back-off reduces power efficiency and may be particularly undesirable for power-sensitive OFDM transmitters. Recent surveys and 6G waveform studies continue to identify PAPR reduction as an important issue for OFDM-based and OFDM-related waveforms [7–9].

To mitigate the high PAPR of OFDM signals, several approaches have been proposed, including amplitude clipping, selected mapping (SLM), active constellation extension, tone reservation, and partial transmit sequence (PTS) techniques [6,7]. Among these methods, PTS is attractive because it can reduce PAPR without deliberately distorting the transmitted signal. In a typical PTS transmitter, the input frequency-domain data block is partitioned into several disjoint sub-blocks. These sub-blocks are transformed into the time domain and then combined with a set of phase rotation factors. The optimal phase vector is selected by minimizing the PAPR of the resulting candidate signal [10,11]. However, as the number of partitions or phase choices increases, the number of candidates grows rapidly, making direct exhaustive search less suitable for low-power real-time hardware.

Recent PAPR-reduction research has further explored machine learning-assisted tone reservation, frequency-selective PAPR control, and OFDM-based integrated sensing and communications (ISAC) waveform optimization [12–14]. These studies show that PAPR reduction remains an active research topic. Nevertheless, many high-performance techniques still require either nonlinear signal modification, repeated candidate generation, iterative optimization, or multiplication-intensive transforms. For low-power transmitters, these operations may increase hardware cost and processing latency.

Precoding-based PAPR reduction provides another way to disperse signal energy before the inverse fast Fourier transform (IFFT). Some early schemes used matrix operations after the IFFT to smooth the time-domain envelope. Although such processing can reduce peaks, it may also disturb subcarrier orthogonality; if the corresponding recovery matrix is poorly conditioned, equalization can amplify the noise and lead to a serious BER degradation. To avoid this problem, later methods mainly used frequency-domain unitary precoding. Discrete cosine transform (DCT), discrete Fourier transform (DFT), and Zadoff–Chu (ZC) precoders have been studied for this purpose because they help reduce coherent peak formation while keeping the transformation reversible at the receiver. However, DCT-, DFT-, and ZC-based schemes rely on trigonometric or complex-valued coefficients and therefore require a relatively large number of real or complex multipliers.

Although many PAPR reduction methods have been reported, three practical requirements are still difficult to satisfy simultaneously. First, the PAPR of the OFDM waveform should be reduced effectively so that the HPA can operate with a smaller input back-off. Second, the PAPR-reduction operation should not destroy the orthogonality of OFDM subcarriers or introduce an ill-conditioned recovery matrix; otherwise, the receiver noise may be significantly amplified and the BER performance may be degraded. Third, the arithmetic structure should be suitable for low-power hardware implementation. This requirement is important for IoT terminals and compact radio nodes, where hardware multipliers usually dominate silicon area, routing complexity, and dynamic power consumption.

Existing methods generally satisfy only part of these requirements. Time-domain smoothing or matrix-based processing can reduce envelope fluctuation, but the corresponding inverse operation may be poorly conditioned and may cause serious BER degradation. Frequency-domain unitary precoding methods preserve reversibility, but conventional DCT-, DFT-, or ZC-based implementations require coefficient multiplications. Moreover, conventional adjacent or block-based PTS partitioning keeps neighboring subcarriers in the same sub-block, which may limit the diversity of the generated PTS candidates.

To address this trade-off among PAPR reduction, arithmetic complexity, and BER reliability, this paper proposes a multiplier-free Dual-Hadamard architecture. The term multiplier-free in this work refers to the additional precoding and PTS phase-weighting operations introduced by the proposed PAPR-reduction module, excluding the common OFDM FFT/IFFT operations required by all compared OFDM systems. The proposed design uses FWHT for frequency-domain precoding and a binary Hadamard codebook for PTS phase weighting, so the main additional precoding and phase-weighting operations are implemented by additions, subtractions, and sign inversions rather than arithmetic multipliers. The proposed method differs from existing FWHT-PTS and DCT-PTS schemes in both structure and design objective. DCT-PTS schemes use DCT precoding to obtain strong PAPR reduction, but the DCT contains real-valued trigonometric coefficients and therefore introduces arithmetic multipliers. Existing FWHT-PTS or Hadamard-PTS schemes usually use Hadamard processing only in one part of the system, such as either the precoding stage or the phase-weighting stage. In contrast, the proposed Dual-Hadamard architecture uses Hadamard-domain operations in both stages: FWHT precoding spreads the input symbols before partitioning, and H-PTS generates candidate signals using binary sign sequences. In addition, the ILP strategy changes the subcarrier-to-sub-block mapping to reduce local correlation concentration within each PTS sub-block. The main contributions of this paper can be summarized as follows:

- A multiplier-free Dual-Hadamard PAPR-reduction architecture is proposed for OFDM transmitters. By replacing multiplication-intensive DCT-type precoding with FWHT processing, the main frequency-domain precoding operation is implemented only by additions and subtractions.
- An interleaved partitioning strategy is introduced after FWHT precoding. Different from conventional adjacent or block-based partitioning, the proposed ILP periodically distributes subcarriers over different sub-blocks, thereby reducing local correlation concentration and increasing the diversity of PTS candidate waveforms.
- A Hadamard-based PTS weighting stage is adopted, where the candidate phase factors are restricted to $\{+1, -1\}$. Therefore, the phase weighting operation is realized by sign retention and sign inversion rather than complex multiplication.
- A receiver recovery and noise analysis is provided. Since the FWHT precoder and the Hadamard de-rotation matrix are unitary operations, the proposed architecture does not introduce an ill-conditioned inverse transformation or additional noise enhancement under ideal side-information recovery.
- A module-level comparison is provided to clarify the incremental contribution of each component, with comprehensive complexity and simulation results demonstrating the proposed performance–complexity trade-off. Compared with the DCT-based benchmark, the proposed method incurs a minor PAPR-reduction loss but completely eliminates arithmetic multipliers from both the precoding and phase-weighting stages.

The rest of the paper is arranged as follows. Section 2 introduces the OFDM signal model and PAPR metrics. Section 3 presents the proposed Dual-Hadamard architecture. Section 4 discusses computational complexity. Section 5 presents the numerical results. Section 6 interprets the results and limitations. Section 7 concludes the paper.

2. System Model and Performance Metrics

2.1. OFDM Signal Model

Consider an OFDM system with N active subcarriers. Let $\mathbf{X} = [X_0, X_1, \ldots, X_{N-1}]^T \in \mathbb{C}^{N\times 1}$ denote the frequency-domain data vector, where each X_k is drawn from a modulation constellation such as quadrature phase-shift keying (QPSK) or quadrature amplitude modulation (QAM). In the mathematical derivation, OFDM modulation is represented by the unitary inverse discrete Fourier transform (IDFT). The corresponding discrete-time OFDM signal is

$$x_n = \frac{1}{\sqrt{N}} \sum_{k=0}^{N-1} X_k e^{j2\pi kn/N}, \quad n = 0, 1, \ldots, N-1. \tag{1}$$

In practical implementation, this IDFT is efficiently realized by an inverse fast Fourier transform (IFFT). Throughout this paper, $\mathbf{F}_N$ denotes the unitary DFT matrix and $\mathbf{F}_N^H$ denotes the corresponding unitary IDFT matrix. The term IFFT is used only when referring to the fast algorithmic implementation of the IDFT.

In practical PAPR evaluation, oversampling is used to better approximate the continuous-time peak value. With an oversampling factor J, the N-subcarrier data vector is mapped into a JN-length frequency-domain vector through zero padding, and the oversampled time-domain signal is denoted by $\mathbf{x}_J = [x_0, x_1, \ldots, x_{JN-1}]^T$. A commonly adopted choice is $J \geq 4$, which provides an accurate approximation of the analog waveform peaks.

2.2. PAPR and CCDF

The PAPR of the oversampled OFDM signal is defined as the ratio between the maximum instantaneous power and the average signal power:

$$\mathrm{PAPR}(\mathbf{x}_J) = \frac{\max\limits_{0 \leq n \leq JN-1} |x_n|^2}{\frac{1}{JN} \sum\limits_{n=0}^{JN-1} |x_n|^2}. \tag{2}$$

For statistical performance evaluation, the complementary cumulative distribution function (CCDF) is widely used. It is defined as the probability that the PAPR exceeds a given threshold PAPR_0:

$$\mathrm{CCDF}(\mathrm{PAPR}_0) = \Pr\{\mathrm{PAPR}(\mathbf{x}_J) > \mathrm{PAPR}_0\}. \tag{3}$$

For large N, the real and imaginary components of an uncoded OFDM signal can be approximated as Gaussian random variables according to the central limit theorem. Consequently, the amplitude is approximately Rayleigh-distributed, and high peaks occur with non-negligible probability. PAPR reduction schemes aim to modify the statistical structure of $\mathbf{x}_J$ while preserving reliable data recovery at the receiver.

3. Proposed Dual-Hadamard Architecture

As shown in Figure 1, the proposed architecture consists of three tightly coupled stages: FWHT precoding, ILP-based sub-block partitioning, and H-PTS weighting. The design objective is not only to reduce the PAPR of OFDM signals but also to preserve the BER performance and simplify the arithmetic structure of the transmitter. The key idea is to use Hadamard-domain operations in both the precoding and the phase-weighting stages. Since Hadamard matrices contain only $+1$ and -1 entries, the corresponding operations can be implemented by additions, subtractions, and sign inversions.

This design differs from conventional DCT or DFT precoded PTS schemes in two aspects. First, the FWHT precoder avoids multiplication by trigonometric or complex exponential coefficients. Second, the H-PTS phase factors are binary signs rather than arbitrary complex rotations. Therefore, the proposed structure removes arithmetic multipliers from the main PAPR-reduction module. In addition, the ILP strategy periodically scatters subcarriers over different sub-blocks, which prevents adjacent frequency components from being concentrated in the same PTS partition and improves the diversity of candidate waveforms.

From an architectural viewpoint, the proposed method can be regarded as a three-stage co-design rather than a direct reuse of a single existing PAPR-reduction block. The FWHT stage performs multiplier-free frequency-domain spreading, the ILP stage changes the subcarrier-to-sub-block mapping to reduce local correlation concentration, and the H-PTS stage generates candidate waveforms through binary sign combinations. Therefore, the novelty of the proposed architecture lies in the joint use of these three operations: FWHT provides multiplier-free precoding, ILP improves the diversity of the PTS sub-blocks, and H-PTS preserves the sign-only candidate-generation structure.

To make the research design explicit, the proposed method is evaluated according to four linked questions: (i) whether the architecture reduces the PAPR relative to conventional OFDM; (ii) whether the unitary recovery structure preserves BER performance in a linear channel; (iii) whether the reduced PAPR improves robustness under nonlinear HPA distortion; and (iv) whether the side-information requirement remains small and can be protected when errors occur. The following subsections define the transmitter processing, receiver recovery, and complexity model used to answer these questions.

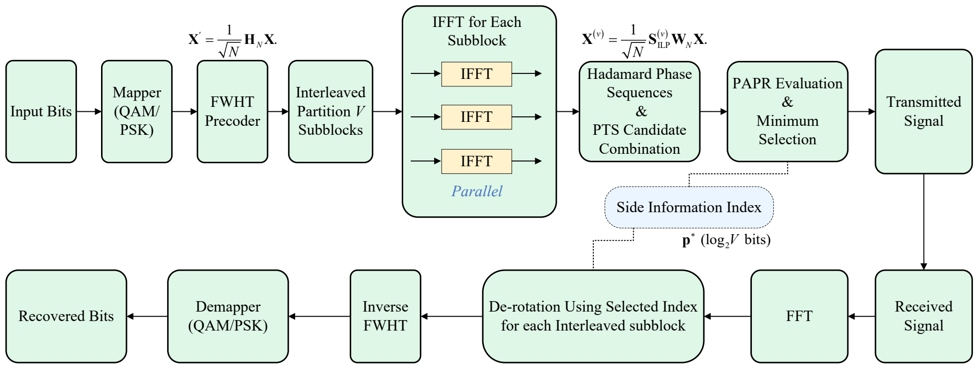

Figure 1. Signal processing flow of the proposed Dual-Hadamard PAPR-reduction architecture. The proposed module consists of FWHT precoding, interleaved partitioning, and Hadamard-sign PTS weighting; the selected candidate index is transmitted as side information for receiver-side de-rotation.

3.1. FWHT Precoding

In conventional precoding-assisted OFDM systems, the input data vector is multiplied by a unitary precoding matrix. If the matrix contains complex exponentials or trigonometric coefficients, this operation introduces a considerable number of hardware multipliers. To avoid this overhead, the proposed method employs a Walsh–Hadamard matrix.

Let $\mathbf{W}_N$ denote the unnormalized Sylvester-type Hadamard matrix of order $N = 2^m$, recursively defined as

$$\mathbf{W}_1 = [1], \quad \mathbf{W}_N = \begin{bmatrix} \mathbf{W}_{N/2} & \mathbf{W}_{N/2} \\ \mathbf{W}_{N/2} & -\mathbf{W}_{N/2} \end{bmatrix}. \tag{4}$$

Its entries are $+1$ or -1, and it satisfies

$$\mathbf{W}_N \mathbf{W}_N^T = N\mathbf{I}_N. \tag{5}$$

The normalized Hadamard matrix is then defined as

$$\mathbf{H}_N = \frac{1}{\sqrt{N}}\mathbf{W}_N, \quad \mathbf{H}_N \mathbf{H}_N^T = \mathbf{I}_N. \tag{6}$$

The precoded frequency-domain vector is

$$\mathbf{X}_{\mathrm{p}} = \mathbf{H}_N \mathbf{X} = \frac{1}{\sqrt{N}} \mathbf{W}_N \mathbf{X}. \tag{7}$$

The core computation $\mathbf{W}_N \mathbf{X}$ can be implemented by FWHT butterflies using only additions and subtractions. The fixed normalization factor $1/\sqrt{N}$ can be merged with the IFFT normalization or absorbed into the transmitter gain control; therefore, it does not require a variable coefficient multiplier in the main signal path.

From a signal-statistical perspective, FWHT precoding linearly combines all input constellation symbols using binary signs. This operation spreads the contribution of each modulated symbol across the frequency-domain vector and reduces the probability that a localized group of subcarriers coherently creates a large time-domain peak. Since $\mathbf{H}_N$ is unitary, the average signal energy is preserved.

3.2. Interleaved Partitioning

After FWHT precoding, $\mathbf{X}_{\mathrm{p}}$ is divided into V disjoint sub-blocks. Let $M = N/V$ denote the number of nonzero subcarriers in each sub-block, and assume that V divides N. In conventional adjacent partitioning, also referred to as CFDP in this paper, adjacent subcarriers are assigned to the same partition. The corresponding selection matrix for the v-th block can be written as

$$\mathbf{S}_{\mathrm{CFDP}}^{(v)} = \mathrm{diag}\left(\mathbf{0}_{(v-1)M}^T, \mathbf{1}_M^T, \mathbf{0}_{(V-v)M}^T\right), \quad v = 1, 2, \ldots, V. \tag{8}$$

Although CFDP is simple and effective, it assigns neighboring subcarriers to the same sub-block. Therefore, it represents an adjacent grouping strategy.

In the proposed architecture, an interleaved partitioning (ILP) strategy is adopted as a structured alternative to adjacent grouping. Define the diagonal selection matrix $\mathbf{S}_{\mathrm{ILP}}^{(v)} = \mathrm{diag}(s_0^{(v)}, s_1^{(v)}, \ldots, s_{N-1}^{(v)})$, where

$$s_k^{(v)} = \begin{cases} 1, & \mathrm{mod}(k, V) = v - 1, \\ 0, & \text{otherwise.} \end{cases} \tag{9}$$

The v-th interleaved sub-block is then

$$\mathbf{X}^{(v)} = \mathbf{S}_{\mathrm{ILP}}^{(v)} \mathbf{X}_{\mathrm{p}}, \quad \sum_{v=1}^{V} \mathbf{X}^{(v)} = \mathbf{X}_{\mathrm{p}}. \tag{10}$$

Unlike CFDP, ILP periodically distributes the selected subcarriers over the whole frequency band. This provides a deterministic non-adjacent subcarrier-to-sub-block mapping for the subsequent H-PTS stage.

3.3. Hadamard-PTS Weighting and PAPR Optimization

Each partitioned sub-block is transformed into the time domain by the unitary inverse discrete Fourier transform (IDFT):

$$\mathbf{x}^{(v)} = \mathbf{F}_N^H \mathbf{X}^{(v)}, \quad v = 1, 2, \ldots, V, \tag{11}$$

where $\mathbf{F}_N$ is the unitary DFT matrix.

In the proposed H-PTS stage, the phase vector $\mathbf{p} = [p_1, p_2, \ldots, p_V]^T$ is selected from a structured Hadamard codebook:

$$\Omega_H = \left\{ \mathbf{p}_u \mid \mathbf{p}_u^T \text{ is the } u\text{-th row of } \mathbf{W}_V,\ u = 1, 2, \ldots, V \right\}. \tag{12}$$

Thus, each phase factor satisfies $p_v \in \{+1, -1\}$. Instead of exhaustively searching all 2^V binary sign combinations, the proposed method uses the V rows of the $V \times V$ Hadamard matrix as a low-complexity structured candidate set. Therefore, the number of candidate phase vectors is $U_H = V$.

For a given phase vector $\mathbf{p}$, define the diagonal phase matrix

$$\mathbf{D}(\mathbf{p}) = \sum_{v=1}^{V} p_v \mathbf{S}_{\mathrm{ILP}}^{(v)}. \tag{13}$$

Under the ILP rule, this matrix can be explicitly expressed in diagonal form as

$$\mathbf{D}(\mathbf{p}) = \mathrm{diag}(d_0, d_1, \ldots, d_{N-1}), \tag{14}$$

where the k-th diagonal entry is given by

$$d_k = p_{(k \bmod V)+1}, \quad d_k \in \{+1, -1\}, \quad k = 0, 1, \ldots, N-1. \tag{15}$$

Therefore, $\mathbf{D}(\mathbf{p})$ is a diagonal sign matrix and satisfies

$$\mathbf{D}^H(\mathbf{p})\mathbf{D}(\mathbf{p}) = \mathbf{I}_N.$$

The candidate time-domain waveform can then be expressed as

$$\tilde{\mathbf{x}}(\mathbf{p}) = \mathbf{F}_N^H \mathbf{D}(\mathbf{p}) \mathbf{H}_N \mathbf{X}. \tag{16}$$

Equivalently, the transmitter implementation first computes the IDFT/IFFT of each partitioned sub-block once:

$$\mathbf{x}^{(v)} = \mathbf{F}_N^H \mathbf{S}_{\mathrm{ILP}}^{(v)} \mathbf{H}_N \mathbf{X}, \quad v = 1, 2, \ldots, V. \tag{17}$$

After these V sub-block waveforms have been obtained, different PTS candidates are generated by a simple time-domain sign-weighted combination:

$$\tilde{\mathbf{x}}(\mathbf{p}) = \sum_{v=1}^{V} p_v \mathbf{x}^{(v)}. \tag{18}$$

Therefore, the sub-block IFFT operations are not repeated for every candidate phase vector. The candidate search is performed entirely via sign changes, time-domain additions, and PAPR evaluation. For oversampled PAPR evaluation in the simulations, frequency-domain zero padding is used to obtain a JN-point waveform. This oversampling step is used only for accurate CCDF estimation and is not counted as an additional PAPR-reduction operation because the common OFDM IFFT/FFT operations are excluded from the complexity comparison.

The optimal phase vector is selected by minimizing the PAPR of the deterministic transmit candidate waveform:

$$\mathbf{p}^\star = \arg\min_{\mathbf{p} \in \Omega_H} \frac{\|\tilde{\mathbf{x}}(\mathbf{p})\|_\infty^2}{\frac{1}{N}\|\tilde{\mathbf{x}}(\mathbf{p})\|_2^2}. \tag{19}$$

It should be noted that this optimization is performed at the transmitter before channel transmission. Therefore, the instantaneous receiver noise is not involved in the PAPR search. The robustness under noise is instead guaranteed by the unitary receiver recovery structure. Since both $\mathbf{D}(\mathbf{p})$ and $\mathbf{H}_N$ are unitary, the selected phase vector modifies the time-domain peak distribution but does not change the average signal energy or introduce an ill-conditioned inverse operation.

For a given phase vector $\mathbf{p}$, the candidate waveform can be written as

$$\tilde{\mathbf{x}}(\mathbf{p}) = \mathbf{F}_N^H \mathbf{D}(\mathbf{p}) \mathbf{H}_N \mathbf{X},$$

where

$$\mathbf{D}(\mathbf{p}) = \sum_{v=1}^{V} p_v \mathbf{S}_{\mathrm{ILP}}^{(v)}.$$

Because $p_v \in \{+1, -1\}$ and the selection matrices $\mathbf{S}_{\mathrm{ILP}}^{(v)}$ are mutually disjoint, $\mathbf{D}(\mathbf{p})$ is a diagonal unitary matrix satisfying

$$\mathbf{D}^H(\mathbf{p}) \mathbf{D}(\mathbf{p}) = \mathbf{I}_N.$$

Thus, changing $\mathbf{p}$ modifies the time-domain peak distribution of the candidate waveform but does not change the average signal energy. The denominator of the PAPR expression is therefore preserved for all Hadamard phase candidates, and the search can be interpreted as selecting the sign pattern that minimizes the maximum instantaneous envelope power.

Under noise interference, the noise does not participate in the transmitter-side PAPR search. The robustness of the proposed architecture is instead guaranteed by the unitary structure of the receiver recovery. Since both $\mathbf{D}(\mathbf{p})$ and $\mathbf{H}_N$ are unitary, the selected phase vector does not introduce an ill-conditioned inverse operation at the receiver. Consequently, the proposed PAPR optimization reduces the peak envelope of the transmitted signal while preserving the noise statistics after ideal de-rotation and inverse FWHT processing.

3.4. Receiver Recovery and Noise Analysis

Let the selected diagonal de-rotation matrix be defined as

$$\mathbf{D}(\mathbf{p}^\star) = \sum_{v=1}^{V} p_v^\star \mathbf{S}_{\mathrm{ILP}}^{(v)} = \mathrm{diag}(d_0^\star, d_1^\star, \ldots, d_{N-1}^\star), \tag{20}$$

where the k-th diagonal entry is $d_k^\star = p_{(k \bmod V)+1}^\star \in \{+1, -1\}$. After cyclic prefix (CP) insertion and transmission over a linear channel, the CP is removed at the receiver. If the CP length satisfies $N_{\mathrm{CP}} \geq L_h - 1$, where L_h is the channel impulse-response length, the linear convolution between the channel and the transmitted signal can be mathematically represented as circular convolution. The received time-domain signal after CP removal can then be expressed as

$$\mathbf{y} = \mathbf{C}_h \mathbf{x}_{\mathrm{opt}} + \mathbf{n}, \tag{21}$$

where $\mathbf{C}_h$ is the circulant channel matrix and $\mathbf{n} \sim \mathcal{CN}(\mathbf{0}, \sigma_n^2 \mathbf{I}_N)$ denotes AWGN. Applying the unitary DFT to (21) gives

$$\mathbf{Y} = \mathbf{\Lambda} \mathbf{D}(\mathbf{p}^\star) \mathbf{H}_N \mathbf{X} + \mathbf{Z}, \tag{22}$$

where $\mathbf{\Lambda} = \mathrm{diag}(H_0, H_1, \ldots, H_{N-1})$ is the channel frequency response diagonal matrix and $\mathbf{Z} = \mathbf{F}_N \mathbf{n}$.

Assuming perfect channel-state information, one-tap frequency-domain equalization yields

$$\hat{\mathbf{X}}_{\mathrm{eq}} = \mathbf{\Lambda}^{-1}\mathbf{Y} = \mathbf{D}(\mathbf{p}^{\star})\mathbf{H}_N\mathbf{X} + \tilde{\mathbf{Z}}, \tag{23}$$

where $\tilde{\mathbf{Z}} = \mathbf{\Lambda}^{-1}\mathbf{Z}$ is the equalized noise vector. With correctly recovered side information, the receiver first applies the inverse Hadamard phase operation and then the inverse FWHT:

$$\hat{\mathbf{X}} = \mathbf{H}_N^T\mathbf{D}^H(\mathbf{p}^{\star})\hat{\mathbf{X}}_{\mathrm{eq}}. \tag{24}$$

Substituting (23) into (24) yields

$$\hat{\mathbf{X}} = \mathbf{H}_N^T\mathbf{D}^H(\mathbf{p}^{\star})\mathbf{D}(\mathbf{p}^{\star})\mathbf{H}_N\mathbf{X} + \mathbf{H}_N^T\mathbf{D}^H(\mathbf{p}^{\star})\tilde{\mathbf{Z}}. \tag{25}$$

Since $\mathbf{D}(\mathbf{p}^{\star})$ and $\mathbf{H}_N$ are unitary matrices, they satisfy the following properties:

$$\mathbf{D}^H(\mathbf{p}^{\star})\mathbf{D}(\mathbf{p}^{\star}) = \mathbf{I}_N, \quad \text{and} \quad \mathbf{H}_N^T\mathbf{H}_N = \mathbf{I}_N.$$

By applying these properties to (25), the recovered signal simplifies to

$$\hat{\mathbf{X}} = \mathbf{X} + \mathbf{H}_N^T\mathbf{D}^H(\mathbf{p}^{\star})\tilde{\mathbf{Z}}. \tag{26}$$

Equation (26) demonstrates that the transmitted data vector $\mathbf{X}$ is recovered without deterministic distortion when the side information is correct. In a linear AWGN channel, or after ideal equalization when the post-equalization noise covariance is proportional to the identity matrix, the recovered noise covariance is expressed as

$$\mathbf{R}_{\hat{\mathbf{Z}}} = \sigma_n^2\mathbf{H}_N^T\mathbf{D}^H(\mathbf{p}^{\star})\mathbf{D}(\mathbf{p}^{\star})\mathbf{H}_N = \sigma_n^2\mathbf{I}_N. \tag{27}$$

Therefore, the FWHT precoding and H-PTS de-rotation do not amplify the noise or change its covariance. The proposed architecture consequently does not introduce inherent BER degradation compared with conventional OFDM in a linear AWGN channel.

This property is fundamentally different from time-domain matrix smoothing methods. In those methods, the receiver must multiply the received signal by the inverse or pseudo-inverse of the smoothing matrix. If the recovery matrix is ill-conditioned, the background noise can be severely amplified, causing a large BER penalty even when the PAPR is reduced. By contrast, the proposed Dual-Hadamard architecture uses only unitary and sign-based transformations, ensuring that the condition number of the recovery operation remains one.

4. Computational Complexity Analysis

To evaluate the hardware efficiency of the proposed method, this section compares the computational complexity of different PAPR-reduction schemes in terms of real multiplications (RMs) and real additions (RAs). The common IFFT/FFT operations required by all OFDM transmitters and receivers are not included in the comparison. The focus is placed on the additional arithmetic cost introduced by the PAPR-reduction module.

4.1. Precoding Stage

For DCT-based precoding, the transform coefficients are real-valued trigonometric constants. A fast one-dimensional DCT applied to a complex input vector can be implemented by separately processing the real and imaginary parts. Its approximate arithmetic complexity is

$$\mathrm{RM}_{\mathrm{DCT}} = N\log_2 N,$$

and

$$\mathrm{RA}_{\mathrm{DCT}} = 3N \log_2 N.$$

Therefore, although DCT precoding can provide good PAPR reduction, it requires a considerable number of coefficient multiplications.

In contrast, the FWHT matrix contains only $+1$ and -1 entries. The corresponding fast transform is implemented by butterfly additions and subtractions. For a complex-valued vector, the required arithmetic complexity is

$$\mathrm{RM}_{\mathrm{FWHT}} = 0,$$

and

$$\mathrm{RA}_{\mathrm{FWHT}} = 2N \log_2 N.$$

The fixed normalization factor $1/\sqrt{N}$ can be merged with the IFFT normalization or absorbed into the digital gain-control stage. Therefore, it does not require a variable-coefficient multiplier in the main signal path.

4.2. PTS Weighting and Candidate Search Stage

In the PTS stage, the complexity depends not only on the number of partitions V, but also on the number of candidate phase vectors. Let U denote the number of candidate phase vectors used by a conventional PTS scheme with arbitrary complex phase rotations.

For one candidate waveform, multiplying V complex-valued sub-blocks by arbitrary complex phase factors requires approximately $4NV$ real multiplications and $2NV$ real additions. Combining the V complex-valued time-domain sub-blocks requires another $2N(V-1)$ real additions. Therefore, for a complete search over U candidate phase vectors, the complexity of conventional arbitrary-phase PTS is formulated as

$$\mathrm{RM}_{\mathrm{PTS}} = 4NVU, \tag{28}$$

and

$$\mathrm{RA}_{\mathrm{PTS}} = 2NVU + 2N(V-1)U. \tag{29}$$

In the proposed H-PTS stage, the candidate phase factors are restricted to $p_v \in \{+1, -1\}$. Thus, the phase weighting operation is implemented by sign retention or sign inversion. No arithmetic multiplier is required for phase rotation. Since the proposed Hadamard codebook contains $U_H = V$ candidate vectors, the arithmetic complexity of the H-PTS candidate combination is expressed as

$$\mathrm{RM}_{\text{H-PTS}} = 0, \tag{30}$$

and

$$\mathrm{RA}_{\text{H-PTS}} = 2N(V-1)U_H. \tag{31}$$

The PAPR of each candidate waveform is then evaluated and the candidate with the minimum PAPR is selected. The comparison operation itself is not included in the arithmetic count because it does not involve real multiplications or additions in the signal-processing datapath.

4.3. Overall Comparison

Table 1 summarizes the transmitter-side complexity of the compared PAPR-reduction modules. The common OFDM modulation/demodulation FFT/IFFT operations are not included, because they are required by all schemes. The table focuses on the additional operations introduced by precoding and PTS candidate generation.

Table 1. Computational complexity comparison of different PAPR-reduction modules, excluding common OFDM FFT/IFFT operations.

Scheme	**Real Multiplications (RMs)**	**Real Additions (RAs)**
Conventional PTS with arbitrary phases	$4NVU$	$2NVU + 2N(V-1)U$
DCT-CFDP-H-PTS	$N \log_2 N$	$3N \log_2 N + 2N(V-1)U_H$
Proposed FWHT-ILP-H-PTS	0	$2N \log_2 N + 2N(V-1)U_H$

This comparison shows that the proposed scheme converts the main PAPR-reduction operations from multiplication-intensive processing to addition/subtraction and sign-operation processing. Such a reduction is significant for FPGA and ASIC implementations, where multipliers usually consume more silicon area and dynamic power than adders and sign inversions. Therefore, the proposed Dual-Hadamard architecture provides a favorable performance–complexity trade-off for low-power OFDM transmitters.

4.4. Comparison with Representative PAPR-Reduction Methods

To further clarify the difference between the proposed architecture and existing PAPR-reduction methods, Table 2 compares several representative schemes in terms of implementation principle, arithmetic feature, side-information overhead, BER impact, and PAPR-reduction characteristic.

Table 2. Qualitative comparison of representative PAPR-reduction methods in terms of implementation principle, arithmetic feature, side-information (SI) overhead, BER impact, and PAPR-reduction characteristic.

Method	**Main Principle**	**Arithmetic Feature**	**SI Overhead**	**BER Impact**	**PAPR Characteristic**
Clipping/companding	Nonlinear amplitude modification in the time domain	Low arithmetic cost	No SI	May introduce in-band distortion and BER degradation	Effective but distortion-based
SLM	Generates multiple alternative OFDM blocks and selects the lowest-PAPR one	Usually requires multiple candidate IFFT operations	$\log_2 U$ bits	Distortionless with correct SI	Good PAPR reduction but high candidate-generation cost
Conventional PTS with arbitrary phases	Partitions the data block and searches over complex phase vectors	Requires complex phase multiplications; about $4NVU$ RMs for candidate phase rotation	$\log_2 U$ bits	Distortionless with correct SI	Good PAPR reduction but search complexity can be high
DCT-CFDP-H-PTS	DCT precoding, adjacent partitioning, and Hadamard PTS weighting	DCT precoder requires about $N \log_2 N$ RMs	$\log_2 U_{\mathrm{H}}$ bits	No inherent BER loss if the unitary recovery and SI are correct	Strong PAPR reduction but multiplication-intensive precoding
Hadamard-PTS only	Uses Hadamard sign sequences for PTS weighting	Multiplier-free phase weighting, but no FWHT precoding	$\log_2 U_{\mathrm{H}}$ bits	No inherent BER loss with correct SI	Moderate PAPR reduction depending on partitioning
Proposed FWHT-ILP-H-PTS	FWHT precoding, interleaved partitioning, and Hadamard sign weighting	Zero RMs in the proposed precoding and phase-weighting stages; additions and sign inversions only	$\log_2 V$ bits when $U_{\mathrm{H}} = V$	No inherent BER loss with correct SI due to unitary recovery	Meaningful PAPR reduction with a multiplier-free arithmetic structure

The comparison shows that the proposed method is positioned as a performance–complexity trade-off. DCT-CFDP-H-PTS may achieve a slightly lower PAPR because the DCT has stronger energy-compaction capability, but it requires multiplication-intensive precoding. SLM can also provide strong PAPR reduction, but it usually requires multiple full-length candidate IFFT operations. By contrast, the proposed FWHT-ILP-H-PTS scheme removes arithmetic multipliers from the additional precoding and phase-weighting stages while preserving the BER performance under correct SI recovery.

5. Simulation Results

This section evaluates the PAPR and BER performance of the proposed Dual-Hadamard scheme. The experiments are organized to address the main concerns of PAPR-reduction design: PAPR reduction, BER preservation, nonlinear-amplifier robustness, multipath-channel applicability, and side-information sensitivity. To improve reproducibility, the key simulation parameters are summarized in Table 3. The main PAPR CCDF and linear AWGN BER simulations are conducted under a QPSK-based OFDM setting. The nonlinear SSPA simulation uses 16-QAM to evaluate the robustness of the proposed scheme under a more amplitude-sensitive modulation format. Additional numerical results are included to provide a table-based module-level PAPR ablation analysis, a frequency-selective Rayleigh fading BER evaluation, and an SI-error sensitivity evaluation.

Table 3. Main simulation parameters used in the numerical evaluation.

Simulation Item	Main Purpose	Parameter Setting
PAPR CCDF comparison	Evaluate PAPR-reduction capability	$N = 256$, $J = 4$, $JN = 1024$, $V = 4$ and 16, $U_{\mathrm{H}} = 4$ and 16, QPSK, PAPR values read at CCDF $= 10^{-3}$
Linear AWGN BER	Verify BER preservation under a linear channel	$N = 256$, $V = 16$, $U_{\mathrm{H}} = 16$, QPSK and 16-QAM, correct SI recovery, no nonlinear HPA distortion
Module-level PAPR ablation	Quantify the incremental contribution of the main modules in tabular form	$N = 256$, $J = 4$, $V = 16$, $U_{\mathrm{H}} = 16$, QPSK, PAPR values read at CCDF $= 10^{-3}$; the table compares original OFDM, grouping-and-kernel, H-PTS only, DCT-CFDP-H-PTS, and the proposed FWHT-ILP-H-PTS
Nonlinear SSPA BER	Evaluate robustness to nonlinear HPA distortion	$N = 2048$, $J = 4$, $JN = 8192$, $V = 16$, $U_{\mathrm{H}} = 16$, 16-QAM, Rapp SSPA model with $p = 10$ and IBO = 3 dB, ideal AGC/Bussgang-equivalent gain compensation, correct SI recovery
Frequency-selective Rayleigh BER	Evaluate performance over a multipath fading channel	$N = 256$, $V = 16$, $U_{\mathrm{H}} = 16$, $J = 4$ for PTS candidate selection, 16-QAM, $N_{\mathrm{CP}} = 16$, exponential power-delay profile, perfect CSI, one-tap MMSE frequency-domain equalization, correct SI recovery
SI-error sensitivity	Evaluate SI overhead, SI protection, and BER impact of SI errors	$N = 256$, $J = 4$, $V = 16$, $U_{\mathrm{H}} = 16$, $N_{\mathrm{SI}} = \log_2 U_{\mathrm{H}} = 4$ bits, QPSK; SI modeled by a binary symmetric channel with $p_{\mathrm{SI}} = 10^{-3}$ and 10^{-2}; repetition protection with $R = 3$ and $R = 5$; additional SI-error sweep at $E_b/N_0 = 12$ dB

In the plotted AWGN and memoryless SSPA simulations, the CP is not explicitly inserted because no multipath delay spread is considered. In the frequency-selective Rayleigh fading simulation, a cyclic prefix with length $N_{\mathrm{CP}} = 16$ is explicitly inserted, which satisfies $N_{\mathrm{CP}} \geq L_h - 1$ for the considered $L_h = 8$ multipath channel. After CP removal, one-tap MMSE frequency-domain equalization is applied with perfect channel-state information.

The SI-error sensitivity simulation is conducted over a linear AWGN channel in order to isolate the BER degradation caused by incorrect SI recovery from fading-induced equalizer noise enhancement or nonlinear HPA distortion. Since the proposed H-PTS codebook contains $U_{\mathrm{H}} = V = 16$ candidate vectors, the SI length is $N_{\mathrm{SI}} = \log_2 U_{\mathrm{H}} = 4$ bits.

5.1. PAPR Reduction Performance

Figure 2 shows the CCDF curves of PAPR for different schemes. The PAPR values are compared at the representative CCDF level of 10^{-3}. In this simulation, the PTS-based schemes are evaluated under two sub-block partition configurations: $V = 4$ and $V = 16$. The original OFDM exhibits a PAPR of approximately 11.0 dB. The grouping-and-kernel benchmark reduces this value to approximately 8.9 dB, but its time-domain smoothing operation may damage subcarrier orthogonality and cause severe BER degradation.

When the sub-block partition count is small ($V = 4$), the DCT-CFDP-H-PTS benchmark and the proposed FWHT-ILP-H-PTS scheme achieve PAPR values of approximately 8.6 dB and 9.8 dB, respectively, representing a performance gap of 1.2 dB. When the partition count scales up to $V = 16$ (with $U_{\mathrm{H}} = 16$ candidate phase sequences), the PAPR of the DCT benchmark decreases to approximately 7.7 dB, while the proposed scheme achieves a PAPR of approximately 8.4 dB.

These results demonstrate that increasing V significantly enhances the PAPR-reduction capability of both methods. Notably, the performance gap between the proposed scheme and the multiplier-heavy DCT benchmark narrows from 1.2 dB at $V = 4$ to only 0.7 dB at $V = 16$. This highlights the favorable scalability of the proposed multiplier-free Dual-Hadamard architecture as the partition count scales up.

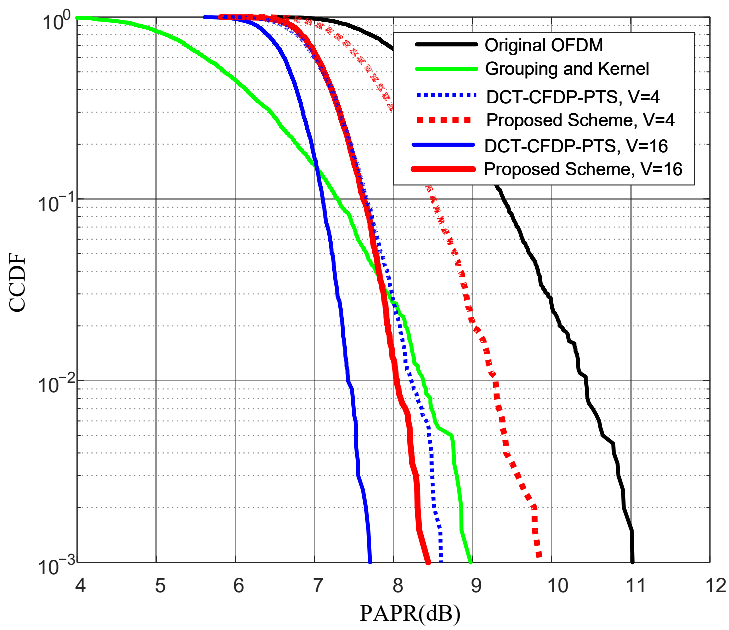

Figure 2. CCDF comparison of PAPR for original OFDM, the grouping-and-kernel benchmark, DCT-CFDP-PTS, and the proposed FWHT-ILP-H-PTS scheme under $V = 4$ and $V = 16$.

5.2. Module-Level Contribution Analysis

To clarify the incremental contribution of each technical component, Table 4 compares several related configurations. The comparison separates the roles of FWHT precoding, ILP, and H-PTS weighting. The PAPR values are reported at CCDF $= 10^{-3}$ using the same simulation setting as Figure 2.

The ablation results indicate that the main PAPR-reduction gain comes from the H-PTS candidate selection. Specifically, the ILP-based H-PTS configuration without transform precoding reduces the PAPR from 11.17 dB to 8.95 dB at CCDF $= 10^{-3}$. After adding

FWHT precoding, the proposed FWHT-ILP-H-PTS scheme further reduces the PAPR to 8.41 dB, which shows the additional contribution of multiplier-free FWHT precoding.

Table 4. Module-level ablation comparison under the same simulation setting.

Scheme	Precoding	Partitioning	Phase Weighting	PAPR at 10^{-3} CCDF
Original OFDM	None	None	None	11.17 dB
H-PTS only	None	ILP	Hadamard signs	8.95 dB
Proposed FWHT-ILP-H-PTS	FWHT	ILP	Hadamard signs	8.41 dB

5.3. BER Performance over a Linear AWGN Channel

Figure 3 compares the BER performance of different schemes over a linear AWGN channel under both QPSK and 16-QAM modulations. The original OFDM curves overlap perfectly with their respective theoretical curves (solid lines for QPSK and dashed lines for 16-QAM), which confirms the correctness of the simulation setup. The DCT-CFDP-H-PTS benchmark and the proposed FWHT-ILP-H-PTS scheme also follow the corresponding theoretical curves precisely in both modulation scenarios. This is because both schemes apply reversible frequency-domain processing and use correct side information for de-rotation.

More importantly, the proposed scheme introduces no observable BER loss compared with conventional OFDM for both low-order (QPSK) and higher-order (16-QAM) modulations. This result agrees with the receiver analysis in Section 3.4. Because the FWHT precoder and the Hadamard phase de-rotation matrix are both unitary operations, the receiver does not require any ill-conditioned inverse operations, and the AWGN covariance is fully preserved after inverse processing. In contrast, the time-domain grouping-and-kernel benchmark exhibits severe BER degradation under both modulations (remaining flat near a BER of 0.4) because its pseudo-inverse recovery matrix is poorly conditioned and significantly amplifies the background noise. These results confirm that the proposed PAPR reduction is achieved without sacrificing the linear-channel BER performance across different modulation formats, provided that the side information is correctly recovered.

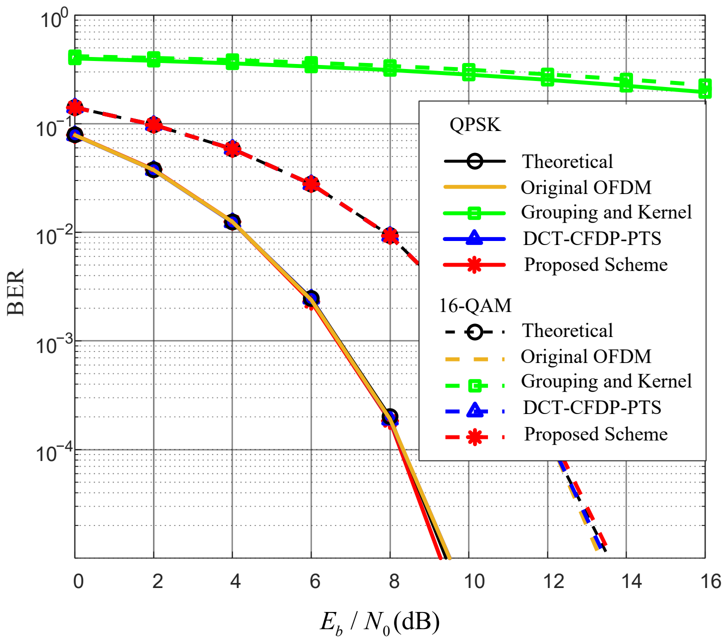

Figure 3. BER performance comparison over a linear AWGN channel under QPSK and 16-QAM modulations.

5.4. BER Performance with Nonlinear SSPA Distortion

The influence of nonlinear amplification is further examined with a solid-state power amplifier (SSPA). The amplitude-to-amplitude (AM/AM) response follows the Rapp model:

$$A(r) = \frac{\alpha r}{\left[1 + \left(\frac{\alpha r}{A_{\text{sat}}}\right)^{2p}\right]^{1/(2p)}}, \quad \Phi(r) \approx 0, \tag{32}$$

where r is the input amplitude, $A(r)$ is the output amplitude, A_{sat} is the saturation amplitude, α is the small-signal gain, and p determines the smoothness of the saturation transition. The AM/PM term $\Phi(r)$ is assumed to be negligible. The simulation uses an input back-off (IBO) of 3 dB and $p = 10$, which corresponds to a strongly nonlinear operating point.

Figure 4 shows the BER performance under nonlinear SSPA distortion using 16-QAM modulation. At low E_b/N_0, the BER performance is mainly limited by AWGN. Therefore, the difference between the original OFDM signal and the proposed scheme is relatively small. As E_b/N_0 increases, the thermal noise becomes weaker, and the nonlinear distortion introduced by the SSPA becomes the dominant impairment. In this high-SNR region, the original OFDM signal suffers from a clear BER floor because its high-PAPR samples are frequently compressed by the nonlinear amplifier.

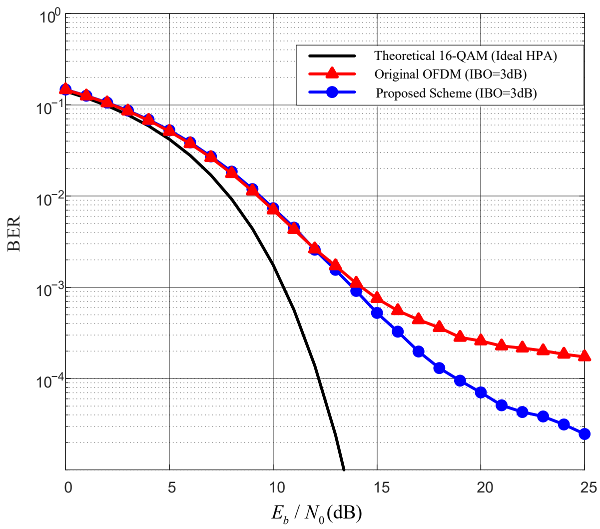

Figure 4. BER performance comparison under nonlinear SSPA distortion modeled by the Rapp model.

The proposed Dual-Hadamard scheme reduces the probability of large envelope peaks before amplification. Consequently, fewer samples enter the nonlinear saturation region, and the residual nonlinear distortion power is reduced. In the receiver, an ideal automatic gain control (AGC) compensation is applied to remove the Bussgang-equivalent linear attenuation caused by the SSPA. However, the nonlinear distortion component cannot be completely removed by AGC. Therefore, the BER advantage of the proposed scheme at high E_b/N_0 comes from suppressing the nonlinear distortion source itself through PAPR reduction. This phenomenon provides an important theoretical implication. PAPR reduction should not be evaluated only by the CCDF curve. Its practical significance is more evident in the distortion-limited high-SNR region, where nonlinear amplifier distortion rather than AWGN dominates the BER performance. The proposed multiplier-free PAPR reduction scheme can therefore improve power-amplifier robustness and suppress the BER error floor without introducing multiplication-intensive signal processing.

5.5. BER Performance over Frequency-Selective Rayleigh Fading Channel

To further examine the applicability of the proposed scheme in a multipath linear channel, a frequency-selective Rayleigh fading channel is considered. In this simulation, 16-QAM modulation is adopted to evaluate the proposed scheme under a more amplitude-sensitive modulation format. A cyclic prefix is explicitly inserted before transmission, and the CP length is set to $N_{\mathrm{CP}} = 16$. The channel length is $L_h = 8$, and therefore the condition $N_{\mathrm{CP}} \geq L_h - 1$ is satisfied.

The channel impulse response is modeled as

$$\mathbf{h} = [h_0, h_1, \ldots, h_{L_h-1}]^T, \quad h_\ell \sim \mathcal{CN}(0, \sigma_\ell^2), \quad \sum_{\ell=0}^{L_h-1} \sigma_\ell^2 = 1, \tag{33}$$

where an exponential power-delay profile is used. After CP removal, one-tap MMSE frequency-domain equalization is performed with perfect channel-state information. The MMSE equalizer for the k-th subcarrier is given by

$$G_k = \frac{H_k^*}{|H_k|^2 + \sigma_z^2}, \quad k = 0, 1, \ldots, N-1, \tag{34}$$

where H_k is the channel frequency response and σ_z^2 denotes the noise variance used in the equalizer. The equalized symbol is then obtained as

$$\hat{X}_{\mathrm{eq},k} = G_k Y_k. \tag{35}$$

Figure 5 compares the BER performance of original OFDM, the grouping-and-kernel benchmark, DCT-CFDP-H-PTS, and the proposed FWHT-ILP-H-PTS scheme over the frequency-selective Rayleigh fading channel. The proposed scheme maintains a comparable BER trend to the DCT-based benchmark under correct SI recovery and perfect CSI. The remaining BER degradation compared with the AWGN case is mainly caused by multipath fading and equalization noise, rather than by the proposed FWHT or H-PTS recovery operations. The grouping-and-kernel benchmark suffers more severe degradation because its receiver recovery relies on a pseudo-inverse matrix, which can further amplify noise after channel equalization.

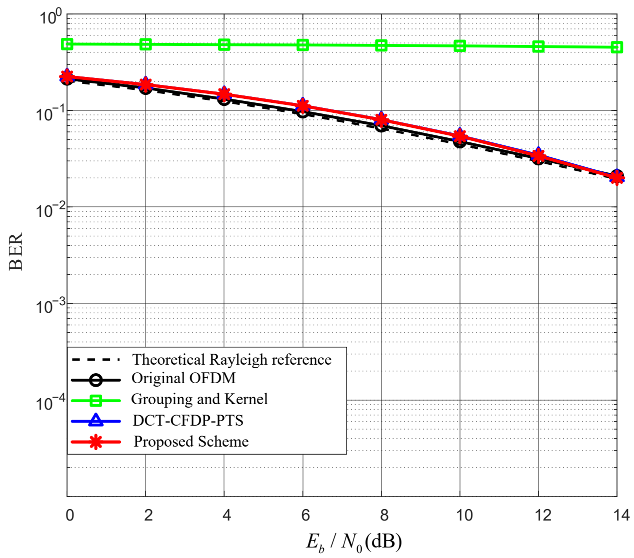

Figure 5. BER performance comparison over a frequency-selective Rayleigh fading channel. The simulation uses 16-QAM, $N = 256$, $V = 16$, $N_{\mathrm{CP}} = 16$, $L_h = 8$, perfect CSI, one-tap MMSE frequency-domain equalization, and correct SI recovery.

5.6. Sensitivity to Side-Information Errors

The previous BER simulations assume correct SI recovery. To evaluate the practical impact of SI errors, an additional SI-error sensitivity simulation is conducted over a linear AWGN channel. The use of an AWGN channel allows the BER degradation caused by incorrect SI recovery to be isolated from fading-induced equalizer noise enhancement and nonlinear HPA distortion.

For the proposed H-PTS codebook, the number of candidate phase vectors is $U_{\mathrm{H}} = V = 16$. Therefore, the SI length is

$$N_{\mathrm{SI}} = \log_2 U_{\mathrm{H}} = \log_2 V = 4 \text{ bits}. \tag{36}$$

For $N = 256$ and QPSK modulation, each OFDM block carries $N \log_2 M_{\mathrm{mod}} = 512$ data bits. Thus, the relative SI overhead is

$$\eta_{\mathrm{SI}} = \frac{N_{\mathrm{SI}}}{N \log_2 M_{\mathrm{mod}}} = \frac{4}{256 \times 2} \approx 0.78\%. \tag{37}$$

In the simulation, the SI bits are modeled as passing through an independent binary symmetric channel with raw SI bit error probability p_{SI}. Both unprotected SI transmission and repetition-protected SI transmission are considered. For an odd repetition factor R, majority decoding is applied at the receiver.

Figure 6 shows the BER performance under ideal SI, unprotected SI errors, and repetition-protected SI. When the SI is correctly recovered, the proposed scheme follows the theoretical QPSK and original OFDM BER trends. When the SI is unprotected, SI bit errors cause incorrect de-rotation and lead to BER degradation, especially at high E_b/N_0, where the data-channel noise becomes small and SI errors dominate. Repetition coding with $R = 3$ or $R = 5$ significantly reduces this degradation.

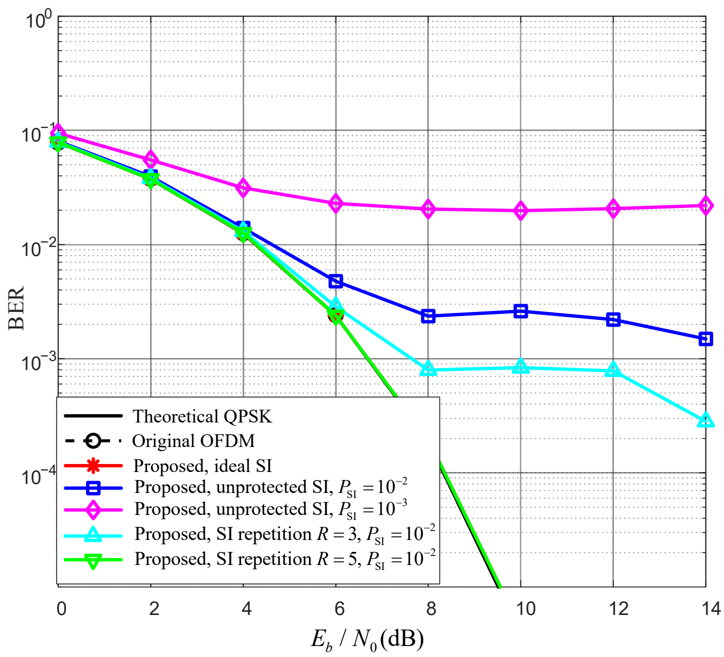

Figure 6. BER performance under SI errors over a linear AWGN channel. The simulation uses QPSK, $N = 256$, $V = 16$, $U_{\mathrm{H}} = 16$, and $N_{\mathrm{SI}} = 4$ bits. The SI bits are modeled by a binary symmetric channel, and repetition protection with $R = 3$ and $R = 5$ is evaluated.

6. Discussion

The simulation results demonstrate that the proposed architecture provides a performance–complexity trade-off for OFDM PAPR reduction. Among the tested PTS-based schemes, DCT-CFDP-H-PTS achieves the lowest PAPR because the DCT has strong energy-compaction capability. However, this improvement requires multiplication-intensive precoding. In contrast, the proposed FWHT-ILP-H-PTS scheme accepts a small PAPR penalty but removes arithmetic multipliers from the additional precoding and phase-weighting stages. Therefore, the proposed method should be understood as a multiplier-free PAPR-reduction architecture rather than a scheme that pursues the absolute minimum PAPR.

The module-level ablation results show that H-PTS candidate selection provides the dominant PAPR-reduction gain compared with original OFDM, while FWHT precoding provides an additional reduction under the multiplier-free structure. The grouping-and-kernel benchmark also reduces PAPR, but its receiver recovery relies on a pseudo-inverse matrix, which may amplify noise and degrade BER. This comparison indicates that PAPR reduction alone is insufficient; the recovery operation should also be well conditioned.

The ILP stage is adopted as a structured non-adjacent subcarrier-to-sub-block mapping within the proposed Dual-Hadamard architecture. Unlike adjacent partitioning, ILP periodically distributes selected subcarriers over the whole frequency band. However, the PAPR performance of a partitioning strategy depends jointly on the precoding transform, the phase candidate set, the number of sub-blocks, and the modulation parameters. Therefore, ILP is not claimed to be universally optimal for all settings. Its role in this work is to provide a deterministic interleaved partitioning structure that is compatible with the proposed FWHT and H-PTS design.

From a BER perspective, the AWGN results confirm that the FWHT precoding and H-PTS de-rotation do not introduce inherent BER degradation when the SI is correctly recovered. This follows from the unitary property of the normalized Hadamard transform and the diagonal sign matrix. Under nonlinear SSPA distortion, PAPR reduction becomes beneficial because it reduces the probability that high-amplitude OFDM samples enter the nonlinear saturation region. Therefore, the BER improvement under SSPA distortion is mainly due to reduced nonlinear distortion rather than a change in modulation or channel coding.

The frequency-selective Rayleigh fading results further verify the proposed scheme under a multipath linear channel with CP insertion, perfect CSI, and one-tap MMSE frequency-domain equalization. The performance degradation relative to the AWGN case mainly comes from fading and equalization noise, rather than from the FWHT or H-PTS recovery operations. The grouping-and-kernel benchmark is more sensitive because pseudo-inverse recovery may further enhance noise after channel equalization.

The proposed architecture is potentially attractive for resource-constrained OFDM transmitters because the additional precoding and phase-weighting operations are implemented without arithmetic multipliers. However, this paper does not provide FPGA or ASIC synthesis results. Therefore, the hardware-related conclusion should be interpreted from the viewpoint of arithmetic operation counts rather than measured silicon area, power consumption, or latency. Practical hardware efficiency also depends on word length, memory access, routing, pipeline design, FFT/IFFT architecture, and implementation technology.

A practical limitation of the proposed H-PTS scheme is the need for reliable side information. Since the Hadamard codebook contains $U_{\mathrm{H}} = V$ candidates, the SI length is

$$N_{\mathrm{SI}} = \log_2 U_{\mathrm{H}} = \log_2 V. \tag{38}$$

For the main setting $V = 16$, only four SI bits are required per OFDM block. Although this overhead is small, these bits are critical because they determine the receiver de-rotation operation.

If the SI is incorrectly recovered, the receiver applies an incorrect phase vector $\hat{\mathbf{p}} \neq \mathbf{p}^{\star}$, and the residual phase operation becomes

$$\mathbf{D}^{H}(\hat{\mathbf{p}})\mathbf{D}(\mathbf{p}^{\star}) \neq \mathbf{I}_{N}. \tag{39}$$

As a result, the recovered data contain deterministic distortion, which may cause a BER floor at high E_b/N_0. The SI-error sensitivity results confirm this behavior and show that simple repetition coding can reduce the degradation. Other practical SI protection methods, such as short block coding, CRC-aided SI detection, reserved pilot subcarriers, or robust low-order SI modulation, can also be considered in future implementations.

The present work also has a limited scope regarding other channel and synchronization impairments. A Rician fading channel can be interpreted as a multipath fading channel with an additional deterministic line-of-sight component; after CP removal and frequency-domain equalization, the proposed FWHT and H-PTS recovery operations remain unitary. Carrier frequency offset and timing synchronization errors are different from linear fading because they directly break OFDM subcarrier orthogonality and introduce inter-carrier interference. These impairments affect conventional OFDM, DCT-precoded OFDM, and the proposed scheme. A complete joint study of PAPR reduction, imperfect synchronization, practical channel estimation, robust SI embedding, and fixed-point hardware implementation is left for future work.

7. Conclusions

This paper proposed a multiplier-free Dual-Hadamard architecture for PAPR reduction in OFDM systems. The proposed scheme integrates FWHT precoding, interleaved partitioning, and Hadamard-based PTS weighting into a unified framework. The FWHT precoder replaces multiplication-intensive DCT-type precoding with addition/subtraction-based butterfly operations. The ILP strategy periodically distributes subcarriers into different sub-blocks, improving the diversity of PTS candidate waveforms. The H-PTS stage restricts the phase factors to $\{+1, -1\}$, so the phase weighting operation is implemented by sign retention and sign inversion rather than complex multiplication.

Theoretical analysis shows that the proposed recovery operation is composed of unitary transformations. With correctly recovered side information, the inverse Hadamard de-rotation and inverse FWHT processing recover the transmitted data without introducing an ill-conditioned inverse matrix. Therefore, the proposed architecture does not cause inherent noise enhancement or BER degradation in a linear AWGN channel.

Simulation results verify the effectiveness of the proposed method. Compared with original OFDM, the proposed scheme significantly reduces the PAPR. Although its PAPR is slightly higher than that of the DCT-based benchmark, this small performance loss is exchanged for the complete removal of arithmetic multipliers from the considered precoding and phase-weighting stages. The BER results over the linear AWGN channel show that the proposed scheme follows the theoretical curve closely. Under nonlinear SSPA amplification, the proposed method suppresses saturation-induced distortion and reduces the BER error floor by lowering the probability of high-envelope peaks.

Overall, the proposed Dual-Hadamard architecture provides a favorable performance–complexity trade-off for resource-constrained OFDM transmitters, especially in low-power IoT scenarios where multiplier-free implementation and amplifier robustness are both important. Future work will focus on fixed-point FPGA/ASIC implementation, robust SI embedding, imperfect channel estimation, and synchronization impairments.

Author Contributions: Conceptualization, M.J. and D.K.; methodology, M.J. and D.K.; software, Y.M. and M.S.; validation, Y.M. and M.S.; formal analysis, M.J.; investigation, M.J.; writing—original draft preparation, M.J.; writing—review and editing, Y.M. and D.K.; supervision, D.K. All authors have read and agreed to the published version of the manuscript.

Funding: This research was funded by the Science and Technology Research and Development Program Joint Fund (Discipline Category) Project of Henan Province, grant number 252301420120, and the Henan Province Postdoctoral Research Project Initiation Fund, grant number HN2022105.

Data Availability Statement: The data presented in this study are available from the corresponding author upon reasonable request.

Conflicts of Interest: The authors declare no conflicts of interest.

References

1. 3GPP. *Release 18 Description; Summary of Rel-18 Work Items*; 3gpp tr 21.918, Version 18.0.0; 3rd Generation Partnership Project: Valbonne, France, 2025.
2. ITU-R. *Framework and Overall Objectives of the Future Development of IMT for 2030 and Beyond*; Recommendation itu-r m.2160-0; International Telecommunication Union: Geneva, Switzerland, 2023.
3. Chen, S.; Liang, Y.C.; Sun, S.; Kang, S.; Cheng, W.; Peng, M. Vision, requirements, and technology trend of 6G: How to tackle the challenges of system coverage, capacity, user data-rate and movement speed. *IEEE Wirel. Commun.* **2020**, *27*, 218–228. [CrossRef]
4. Lu, S.; Liu, F.; Li, Y.; Zhang, K.; Huang, H.; Zou, J.; Li, X.; Dong, Y.; Dong, F.; Zhu, J.; et al. Integrated Sensing and Communications: Recent Advances and Ten Open Challenges. *IEEE Internet Things J.* **2024**, *11*, 19094–19120. [CrossRef]
5. Nguyen, D.C.; Ding, M.; Pathirana, P.N.; Seneviratne, A.; Li, J.; Niyato, D.; Dobre, O.; Poor, H.V. 6G Internet of Things: A comprehensive survey. *IEEE Internet Things J.* **2021**, *9*, 359–383. [CrossRef]
6. Jiang, T.; Wu, Y. An Overview: Peak-to-Average Power Ratio Reduction Techniques for OFDM Signals. *IEEE Trans. Broadcast.* **2008**, *54*, 257–268. [CrossRef]
7. da Silva, B.S.d.C.; Souto, V.D.P.; Souza, R.D.; Mendes, L.L. A Survey of PAPR Techniques Based on Machine Learning. *Sensors* **2024**, *24*, 1918. [CrossRef] [PubMed]
8. Park, M.; Choi, J. Survey on PAPR Reduction: From Signal Processing to Machine Learning-based Techniques. In *Proceedings of the 2025 16th International Conference on Information and Communication Technology Convergence (ICTC)*; IEEE Computer Society: Washington, DC, USA, 2025; pp. 1497–1502. [CrossRef]
9. Liu, J.; Hou, X.; Liu, W.; Li, C.; Chen, L. Low-PAPR 6G Waveform and Modulation Design with 5G NR Backward Compatibility. *IEICE Trans. Commun.* **2026**, *E109.B*, 231–244. [CrossRef]
10. Cimini, L.J.; Sollenberger, N.R. Peak-to-Average Power Ratio Reduction of an OFDM Signal Using Partial Transmit Sequences. *IEEE Commun. Lett.* **2000**, *4*, 86–88. [CrossRef]
11. Jawhar, Y.A.; Audah, L.; Taher, M.A.; Ramli, K.N.; Shah, N.S.M.; Musa, M.; Ahmed, M.S. A Review of Partial Transmit Sequence for PAPR Reduction in the OFDM Systems. *IEEE Access* **2019**, *7*, 18021–18041. [CrossRef]
12. Wang, B.; Si, Q.; Jin, M. A Novel Tone Reservation Scheme Based on Deep Learning for PAPR Reduction in OFDM Systems. *IEEE Commun. Lett.* **2020**, *24*, 1271–1274. [CrossRef]
13. Gökceli, S.; Levanen, T.; Riihonen, T.; Renfors, M.; Valkama, M. Frequency-Selective PAPR Reduction for OFDM. *IEEE Trans. Veh. Technol.* **2019**, *68*, 6167–6171. [CrossRef]
14. Rexhepi, G.; Ranasinghe, K.R.R.; de Abreu, G.T.F.; González, G.D. Tone Reservation-Based PAPR Reduction Using Manifold Optimization for OFDM-ISAC Systems. In *Proceedings of the 2025 IEEE Wireless Communications and Networking Conference (WCNC)*; IEEE: Piscataway, NJ, USA, 2025; pp. 1–6. [CrossRef]

Disclaimer/Publisher's Note: The statements, opinions and data contained in all publications are solely those of the individual author(s) and contributor(s) and not of MDPI and/or the editor(s). MDPI and/or the editor(s) disclaim responsibility for any injury to people or property resulting from any ideas, methods, instructions or products referred to in the content.